極東ネパールヒマラヤ優白質花崗岩の高精度 CHIME モナザイト年代（予報）
High-precision CHIME monazite age from leucogranites in far-eastern Nepal Himalaya (forecast)

今山武志[1*]・鈴木和博[1]
Takeshi Imayama[1*]・Kazuhiro Suzuki[1]

[1]名古屋大学年代測定総合研究センター
[1]Center for Chronological Research, Nagoya University, Chikusa, Nagoya 464-8602, Japan.

Corresponding author. E-mail: imayama@nendai.nagoya-u.ac.jp

Abstract

Monazites, approximately [(LREE,Th,U,Ca)(P,Si)O_4], from two leucogranite samples in far-eastern Nepal Himalaya were dated by the chemical U-Th-total Pb isochron method (CHIME). Monazites in foliated biotite leucogranite exhibit significant chemical characteristics by different grains or within individual grains. Some monazite grains have strongly undergone the chemical alteration through the monazite-huttonite substitution (P^{5+} +REE^{3+} ↔Si^{4+} + Th^{4+}). Other grains, especially surrounding feldspars, have slightly occurred the monazite-cheralite substitution (2REE^{3+} ↔ Ca^{2+} +Th^{4+}), and have the relatively higher concentrations of ThO_2, compared to the huttonite-rich monazite. Furthermore, a significant intra-crystal chemical zoning is observed in individual monazite grains, indicating that Y content decreases from core and to rim. Monazites selected using chemical criteria (0.95 < (Ca + Si)/ (Th + U +Pb +S) < 1.05), which could be discriminate the metamict monazite due to the destruction of the crystalline structure from the original monazites, construct together a pseudo-isochron of 16.4 ± 1.7 Ma in PbO-ThO_2^* diagram. Also, monazites from quartz-rich leucogranite have homogenous compositions of Y, Th and U contents, and yields the weight mean chemical ages of 16.6 ± 2.6 Ma, in agreement with the age of the foliated biotite leucogranite. Our data suggest that the CHIME ages combined with the chemical zoning patterns such as Y, Th, U, Ca, and Pb of monazites can provide a powerful tool to elucidate the complex zoning patterns of monazite and to know the precise timing of granite crystallization from magmatic monazite.

Keywords: Chemical age; Monazite; Himalaya leucogranite

1. Introduction

Monazite dating using the electron probe microanalyser (EPMA) has become increasingly popular since the beginning of the 1990s, especially as a method for constraining the ages of magmatism and metamorphism (Suzuki and Adachi, 1991; Suzuki et al., 1994; Montel et al., 1996; Pyle et al., 2005). The EPMA dating easily allows the age determination by c. 3-5 μm spot size in monazite grain, and the high spatial resolution is a great advantage over other microprobe dating, because monazite grains commonly exhibit complex internal zoning of composition and age on a micrometer scale (e.g. Williams et al., 2007 and

reference there in). The chemical Th-U total-Pb isochron method (CHIME) age using precise EPMA analysis is determined by measuring many spots with compositional variations in monazite crystal, and then by constructing a pseudo-isochron of domains that have constant age within analytical error, assuming that their concentrations have not been significantly lost by subsequent thermal event (Suzuki and Adachi, 1991; Suzuki and Kato, 2008).

Recent studies on monazite geochronology have mainly focused on the correlation of the age and its textural-chemical characteristics on individual or different grains of monazites (e.g. Harrison et al., 2002). In terms of monazites in the Himalayan migmatites and leucogranites, some workers have reported a strong correlation between the ages and Yttrium zoning in monazite crystals, assuming that the Y content in the monazite is mainly controlled by reactions involving garnet (Foster et al., 2000, 2002; Kohn et al., 2005; Cottle et al., 2009). However, another workers have emphasized that the hydrothermal alternation on cooling could be also disturbed the U-Th-Pb geochronometer in monazite (e.g. Townsend et al., 2000; Bollinger and Janots, 2006), in which alternation may occur on the micron to submicron scale smaller than analytical volumes for in-situ dating techniques (Berger et al., 2008). Thus, in order to obtain reliable and accurate ages, it is essential to understand how fluid-assisted metasomatic processes influence chemical compositions in a single monazite crystal or over the grain-scale. Indeed, because Yttrium is not a direct indicator of metamict monazite, the age interpretation cannot be follow by the chemical map of Yttrium alone without knowledge of the internal zoning of the other elements such as Th, U, Ca, P, and Pb in grains.

Here we report the CHIME age and X-ray multiple chemical mapping of monazites from leucogranites in the far-eastern Nepal Himalaya, and constrain the characterization of intra-crystalline variations with the bulk-rock chemistry. The construction of pseudo-isochron by the distinct chemical domains in monazites could contribute to understand the correlation between ages and chemical compositions in the crystal, and the precise CHIME monazite dating.

2. Himalayan leucogranite and sample descriptions

The Himalayan leucogranite is regarded as one of the best example of young S-type leucogranites originating from crustal melting after the Indian - Asian collision (e.g. Le Fort, 1975). In eastern Nepal, the U-Th-Pb ages of monazites and zircons from the leucogranite have been mostly dated at c. 24-16 Ma, using the isotope dilution thermal ionization mass spectrometry (ID-TIMS) on individual grains that were physically separated (Schärer 1984; Copeland et al., 1988; Hodges et al., 1998; Simpson et al., 2000; Viskupic and Hodges, 2001; Viskupic et al., 2005), or the secondary ion-mass spectrometry (SIMS) microanalysis of spots on different grains in thin section (Harrison et al. 1999; Murphy and Harrison 1999; Catlos et al. 2002).

The Kanchenjunga leucogranites in far-eastern Nepal contain the assemblage of biotite + muscovite + quartz + K-feldspar + plagioclase ± tourmaline ± garnet ± sillimanite (Schelling, 1992; Goscombe et al., 2006). The leucogranite bodies occur at various scales, ranging from a few centimeter-sized sills and dikes to several kilometer-sized plutons (e.g. Hodges, 2000). Both foliated and massive leucogranites in thickness within a few meters are frequently intercalated with the migmatites. The protolith of these leucogranites has been generally considered as the base of the amphibolite-facies metasediments, especially on the mica-rich schist, of the Higher Himalayan Crystalline Sequences (HHCS), based on the peraluminous compositions of leucogranites and the similarities in Nd and Sr isotopic ratios between the leucogranite and the metasediments (e.g. Inger and Harris, 1993).

Two samples L02 and L06 were collected from small-volume leucogranitic body (meter-wide sheets and dikes of granite and pegmatite) that occurs at c. 0.5 km east of the Ghunsa town in far-eastern Nepal (Fig. 1). Both samples are foliated biotite leucogranites with mineral assemblages of biotite, fibrolitic sillimanite, plagioclase, quartz and K-feldspar, and it is layered at the micrometer scale, alternating with feldspar-rich leucocratic and mica-rich layers. Biotites are replaced by retrogressive chlorite to varying degrees, which alteration is more pronounced for sample L06 than sample L02. Fibrolitic sillimanite mainly occurs as the fine-grained fibrolite + biotite aggregate at the edge of coarse-grained biotite or fills by itself a crack along the grain boundary or within the crystals.

Four leucogranite samples L01, L03, L05, and L07 were corrected from the floats at the Kanchenjunga basecamp, which samples may be expected as the parts of the plutonic rocks of the Jannu Granites (Fig. 1). Sample L05 is fine-grained massive granite, and almost consist of quartz with minor amounts of biotite, muscovite, fibrolite and feldspars. Thin films of fibrolitic sillimanite mainly occur along the grain boundary of quartz, which could not have reacted with monazite. Samples L01, L03 and L07 are weakly foliated biotite leucogranites, and consist mainly of biotite, muscovite, plagioclase, quartz and K-feldspar with minor fibrolite. Samples L01 and L07 also contain garnet, and the presence of garnet coexisted with K-feldspar in leucogranites suggests that the melting reaction was a vapor-absent biotite dehydration melting reaction such as Bt + Als + Qtz = Grt + Kfs + melt (Imayama et al., 2010). Small garnet and the rims of large porphyroblasts were replaced by the retrograde assemblage such as fibrolite and biotite following the later chlorite. Sample L01 is tourmaline-rich and mica-poor leucogranite, and does not include garnet.

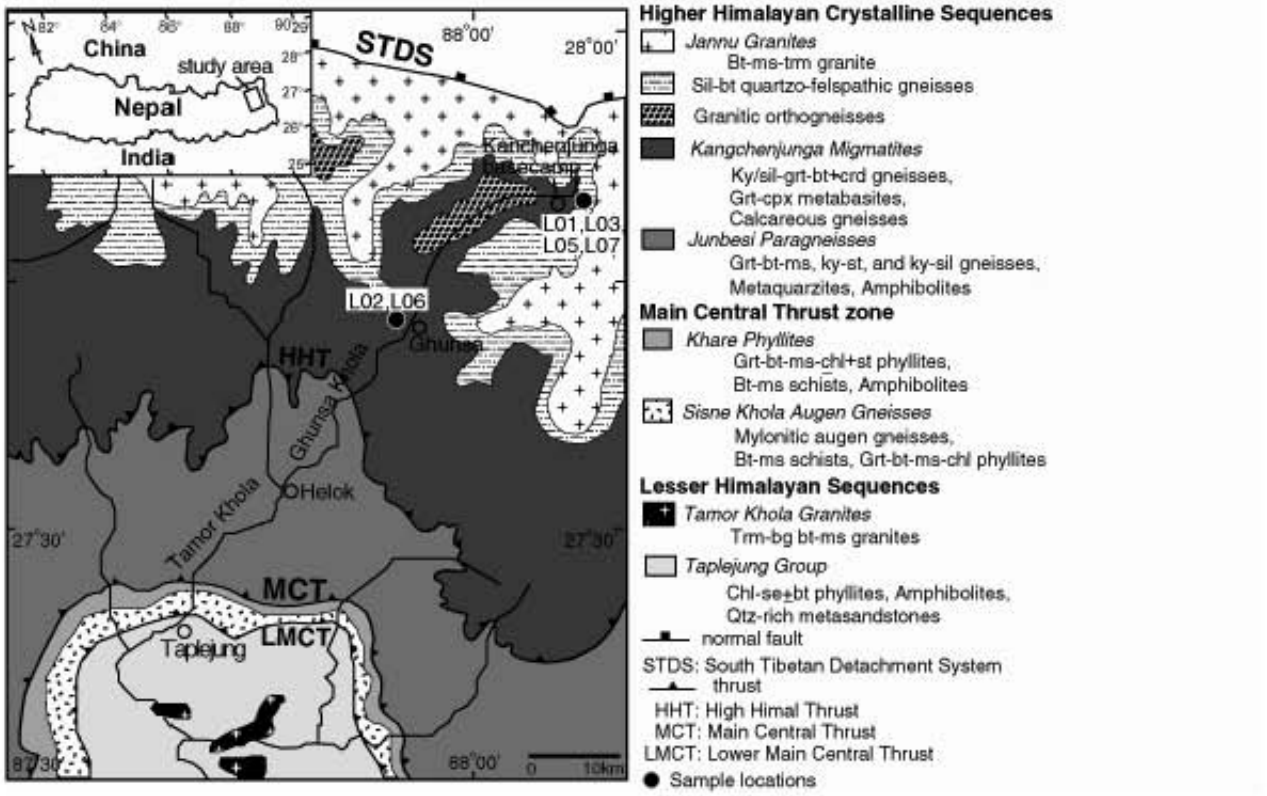

Fig. 1. Simplified geological map of far-eastern Nepal, showing location of samples used for CHIME dating (solid circles). Abbreviations. Bt: biotite; Ms: muscovite; Trm: tourmaline; Ky: kyanite; Sil: sillimanite; Grt: garnet; Crd: Cordierite; Cpx: clinopyroxene; Chl: chlorite; St: staurolite; Se: Sericite; Qtz: quartz; Kfs: K-feldsper.

3. Whole-rock compositions

Whole-rock compositions were analyzed with a SHIMADZU XRF1800 wavelength dispersive sequential X-ray fluorescence spectrometer with an end-window 4kW Rh X-ray tube at Nagoya University. 100 to 200 g samples were crushed by pounding the blocks with a hammer, and then powdered using the steel mortar. After drying in an oven heated to 110 ℃ for 24 hours, they were mixed with anhydrous lithium tetraborate (0.7 g sample and 6 g flux for analysis of major elements and 2 g sample and 3 g flux for trace elements) and fused with a $Pt_{90}Au_{10}$ crucible in an electric furnace to make the glass bead. The analytical procedure followed those of Morishita and Suzuki (1993). The tube currents for major and trace elements were 70 mA and 95 mA with tube voltage of 40 kV, respectively. The detection limits were 10 ppm for Ba and 0.5-2 ppm for other trace elements at the 2 σ confidence level.

The $Al_2O_3/(CaO+Na_2O+K_2O)$ values for all leucogranite samples range from 1.55-1.93, and the high peraluminous values are characteristics of the S-type granitoids (e.g. Clarke, 1992). The SiO_2 contents are 77.0-71.2 wt% for five leucogranites except for 95.4 wt. % of quartz-rich leucogranite L05. In Harker plots for major elements, Al_2O_3 (16.2–2.7 wt. %), CaO (1.7–0.2 wt. %), Na_2O (5.9–0.3 wt. %), K_2O (5.4–0.9 wt. %) and P_2O_5 (0.14–0.01 wt. %) contents show a marked decrease with increasing SiO_2 content. The low contents of CaO in leucogranites could be suitable for monazite crystallization (e.g. Montel, 1993). Total alkalis for most samples are variable of 8.6-6.7 wt. %, and the high K_2O/Na_2O ratios (3.00–0.73) represent that the rocks belong to the S-type granites via mica dehydration reaction if the protolith doesn't include K-feldspar (Le Breton and Thompson, 1988). Sample L02 has very low alkalis of 1.2 wt. % with low K_2O/Na_2O ratio of 0.20, simply because it could attribute to the small amount of mica. Also, MnO (0.07–0.02 wt. %), MgO (1.0–0.3 wt. %), Fe_2O_3 (3.6–1.8 wt. %), and TiO_2 (0.8–0.2 wt. %) contents, principally hosted by biotite, show no systematic relation with SiO_2 content.

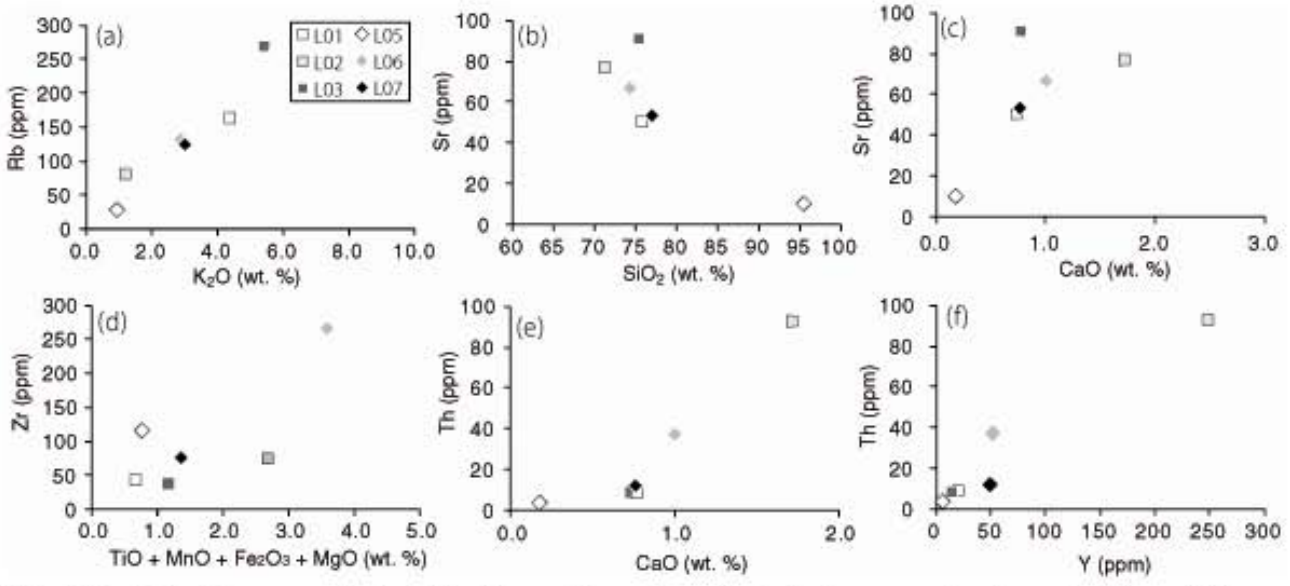

Fig. 2. Variation diagrams of selected major and trace elements in the leucogranites along the Tamor-Ghunsa section. (a) Rb vs. K_2O diagram, (b) Sr vs. SiO_2, (c) Sr vs. CaO, (d) Zr vs. $TiO+MnO+Fe_2O_3+MgO$ diagram, (e) Th vs. CaO diagram, and (f) Th vs. Y diagram.

The Rb contents of the incompatible LILE elements are enriched in leucogranites that have the high K_2O contents (Fig. 2a). The Sr contents decrease with the decreasing of SiO_2 (Fig. 2b), and increase with the

increasing of CaO (Fig. 2c), suggesting plagioclase fractionation. The Nb of immobile high-field-strength elements are below the detection limits in analyzed all samples. The Zr contents for samples L01,L02, L03, L04, and L05 are moderate of c. 40-117 ppm, and sample L06 is relatively higher Zr content of c. 270 ppm and TiO + MnO +Fe_2O_3 + MgO (Fig. 2d). Feldspar-rich sample L02 is characterized by the higher CaO, Th and Y contents, compared with the other leucogranites (Fig. 2e, 2f). Yttrium contents (4-250 ppm) are positively correlated to the Th contents (c. 5-90 ppm), implying that their behaviors in granites are mainly controlled by the amounts and fractionation of monazite (e.g. Montel et al., 1993) or xenotime (e.g. Viskupic and Hodges 2001).

4. CHIME dating and compositional mapping of monazites

Chemical analyses of monazite were performed in-situ on the polished thin section using a JEOL JCXA-733 electron microprobe (EPMA) at Nagoya University with 4 wavelength-dispersive spectrometers, equipped with PET crystals and sealed Xe X-ray detectors. Spot analysis using c. 3-5 μm probe diameter was operated at an accelerating voltage of 15 kV and prove current of 0.2 μA. The X-ray intensity data were converted into concentrations through the procedure of Bence and Albee (1968) with the α-factor table of Kato (2005). Counting times on peak for the analysis of U, Th, Pb and Y were over a 400 s period for the line peak positions and over a 200 s period for two optimum background positions above and below each line peak. For the analyses of other elements, X-ray intensities were integrated over 40 s on peak positions and 20 s on two background positions. UMβ, ThMα, PbMα,YLα, CaKα, SKα, KKα, ZrLα, SiKα and NbLβ lines were simultaneously measured. For X-ray mapping of monazite, a prove current of 300-500 nA, a pixel step of 2-4 μm, and the dwell time per pixel of 10 s were used. The calculation of the CHIME ages and the correction of interferences among the analyzed elements follow the procedure described by Suzuki and Adachi (1991) and Suzuki and Kato (2008). The pseudo-isochron is constructed from the regression line on the PbO–ThO_2 * diagram (ThO_2 * refers to the sum of ThO_2 and the ThO_2 equivalent of UO_2), and obtained both initial PbO content and age (Suzuki and Adachi, 1991).

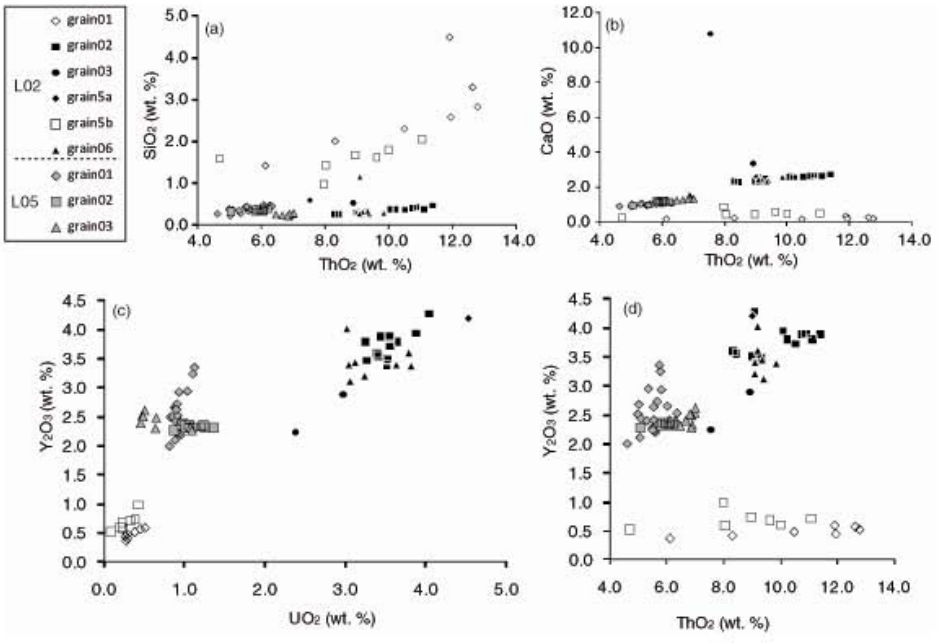

Fig. 3. Variations of (a) SiO_2-ThO_2 contents, (b) CaO-ThO_2 contnts, (c) Y_2O_3-UO_2 contents, and (d) Y_2O_3-ThO_2 contents in analyzed monazite from leucogranites in-far-eastern Nepal. Data of different monazite grains are plotted as shown in legends.

4.1. Sillimanite-bearing biotite-muscovite leucogranite (L02)

Monazite grains from sample L02 commonly exhibit complex textures, primarily due to partial enrichment or depletion in both huttonite ($ThSiO_4$) and cheralite [$CaTh(PO4)_2$] depends on grains. Some monazite grains, which mainly occur at the place spatially associated with the retrograde-stage minerals in thin section, have strongly undergone the chemical reaction through the monazite - huttonite substitution (P^{5+} +REE^{3+} ↔Si^{4+} + Th^{4+}), shown by the correlation of SiO_2 and ThO_2 (Fig. 3a). The ThO_2 from other grains, especially surrounding feldspars, are positively correlated with CaO (Fig. 3b), indicating the monazite - cheralite substitution ($2REE^{3+}$ ↔Ca^{2+} +Th^{4+}), and their grains have the relatively higher concentrations of ThO_2, compared to the huttonite-rich monazite. Also, representative monazite grains from sample L02 can be divided into two zones on the basis of Y content (Fig. 4). The core is characterized by high concentrations of Y, and is surrounded by the rim domain that shows relatively low concentration of Y. The Th content could be basically similar trend of the Y content, but shows a partly patchy zoning related to a relatively variation in P, Ca, and U contents. The U concentrations are relatively uniform across the interior of the grains and decrease clearly in the outermost rims where Th zoning pattern increases. Monazite grains contain micro-inclusions (c. 1–5 μm) of apatite and Th silicate.

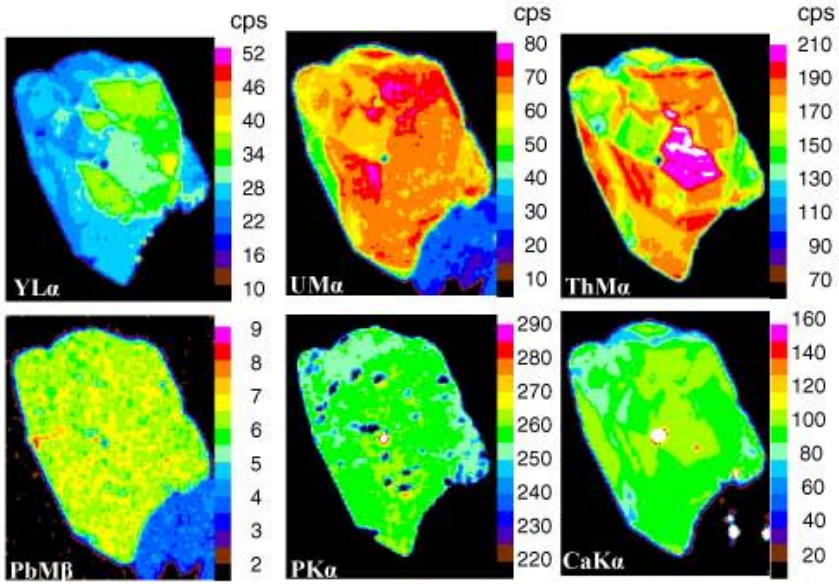

Fig. 4. Compositional mapping images of monazite grains in foliated biotite leucogranite L02 in far-eastern Nepal.

The weighted mean age of 39 analyzed points in six grains is 16.4 ± 1.7 Ma (2σ, MSWD = 0.37). The PbO vs. ThO_2^* plots of monazite is shown in Fig. 5a. Nine data that are not satisfied with the chemical criteria of 0.95 < (Ca + Si)/ (Th + U +Pb +S) < 1.05 are excluded from the isochron calculation, because the stoichiometric constrain for the monazite is strongly broken.

4.2. Quartz-rich leucogranite (L05)

The internal structures of the monazites from quartz-rich leucogranite show irregularly-shaped, but display little or no chemical zoning of Y_2O_3, UO_2, and ThO_2 (Fig. 3c, 3d). The concentrations of Y_2O_3 and ThO_2 in the monazites are higher than huttonite-rich monazite and lower than cheralite –rich monazite in sample L02. The single CHIME age of thirty nine monazite grains were calculated, and the weighted mean age of 39 analyzed points in six grains is 16.6 ± 2.6 Ma (Fig. 5b, 2σ, MSWD = 1.2), statistically in agreement with the isochron age of sample L02.

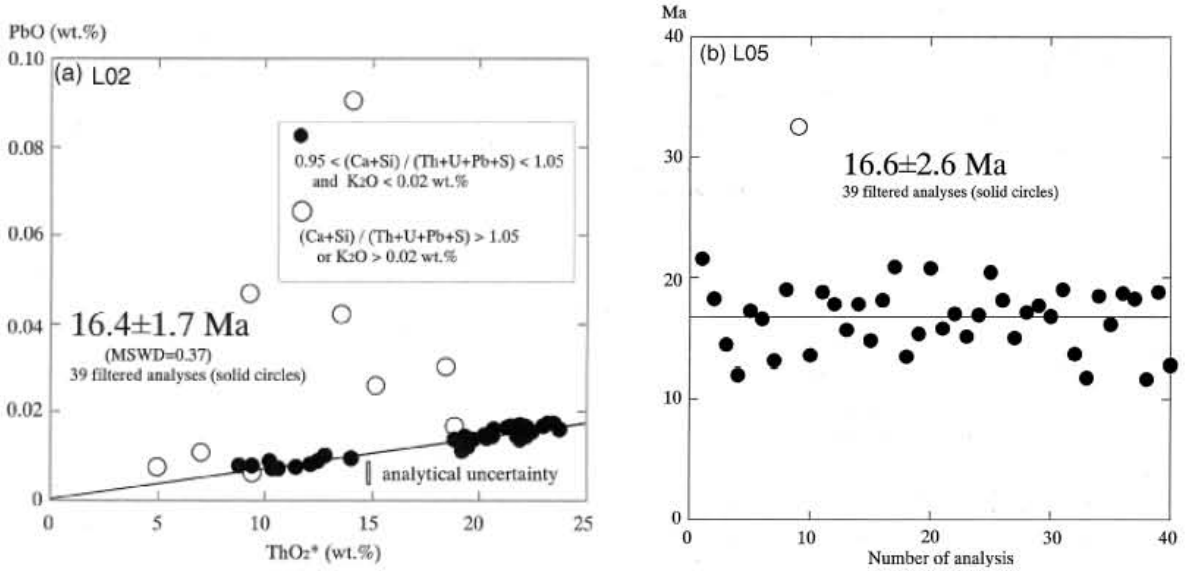

Fig. 5. (a) PbO vs. ThO_2* plots of monazite grains in foliated biotite leucogranite L02. The data selected and rejected using chemical criteria are shown by the solid and open circles, respectively. An isochron age is quoted at 2σ confidence level. (b) The weighted mean CHIME age (2σ) of quart-rich leucogranite L05.

5. Discussion

The CHIME dating has assumed that (1) initial PbO is negligible in comparison with radiogenic Pb in monazite, and (2) the Th-U-Pb system is not disturbed by the post-solidification thermal events. The successful construction of pseudosection at 16.4 ± 1.7 Ma in monazite grains in sample L02 is likely that the first assumption could be valid. Also, the chemical criteria such as 0.95 < (Ca + Si)/ (Th + U +Pb +S) < 1.05 could possibly discriminate the metamict monazite due to the destruction of the crystalline structure from the original monazites (Suzuki and Kato, 2008), resulting in the more precise CHIME age. In the case of monazites in sample L05, the data rejected using chemical criteria is just only one, indicating that the monazites seem to have escaped from the alteration event, as also shown by the absence of retrograde minerals in thin section. Because it is difficult to construct the pseudosection for homogenous compositions in monazites, the weighted mean age smaller than the error on individual spot age analysis is applied for monazites in sample L05. The monazite CHIME ages of c. 17-16 Ma from both leucogranites have produced the same age as the SHRIMP ages (c. 18-16 Ma) of zircons from the leucogranites along the Tamor-Ghunsa section, far-eastern Nepal (Imayama et al., 2011 in submit), and their ages represent the timing of the melting at c. 18-16 Ma.

The leucogranites in far-eastern Nepal was inferred to have partly formed during biotite dehydration melting of Bt + Als + Qtz = Grt + Kfs + melt (Imayama et al., 2010). Because the peraluminous melt increases phosphorus solubility (Wolf & London, 1994), the monazite generation and dissolution are expected to occur during their melting reactions. Some monazite grains in sample L02 are characterized by the decreasing Y towards their rims, and its zoning could be explained if garnet is produced during melt generation, because the Y partition for garnet and melt are high as well as monazite (e.g. Spear and Pyle, 2002). The xenotime that contains sample L02 could be main reservoir of Yttrium before melting. On the other hand, in the case of partial replacement of monazite by huttonite, the fluid-assisted dissolution - reprecipitation on cooling is also possible mechanism, based on experiments (Harlov et al., 2007). Thus, the Th contents in some monazite grains might decrease resulting from the

breakdown of monazite to thorite via huttonite substitution. Y content in monazite grains from sample L02 is mainly correlated to the U content, rather than the Th content. This is because the monazite cannot replace the U.

In general, monazite gives concordant U–Pb and Th–Pb ages in the case that the concentration of U in monazite is enough high to analyze. However, Schärer et al. (1984) reported the discordant age of young igneous monazite in eastern Nepal, which reflects incorporation of excess ^{230}Th during crystallization, leading to an excess of ^{206}Pb. More recently, the ^{206}Pb/^{238}U ages of monazites using LA-ICP-MS are older than the ^{208}Pb/^{232}Th ages by up to c. 50% (Cottle et al., 2009). The principle advantage of ^{232}Th-^{208}Pb over U-Pb systems for dating Tertiary monazite is a rapid attainment of equilibrium and high Th concentrations, resulting in very high level of ^{208}Pb (Montel, 1993; Harrison et al., 1999). Although the CHIME ages cannot be directly assessed the discordant problem (i.e. isotope), it must be also noted that the even spot size of c. 10-15 μm for ion microprobe is too large to elucidate the complex zoning in monazite grains, as shown by the chemical zoning of monazite in far-eastern Nepal. For Th-rich minerals (e.g., monazite) that preferentially incorporate Th relative to U during growth, ^{206}Pb/^{238}U dates are older than the crystallization age (Crowly et al., 2009).

Acknowledgements

I wish to thank to T. Kato and their colleagues (Nagoya University) for useful discussion on this study. I wish to express my sincere thanks to T. Kajizuka (Nagoya University) for assisting us for XRF analyses. The detailed chemical data of monazite with further discussion for leucogranites in far-eastern Nepal will be published in the American Mineralogist or one of the other international journals in near future.

References

Bence, A.E., Albee, A.L., 1968. Empirical correction factors for the electron microanalysis of silicates and oxides: J. Geology 76, 382-403.

Berger, A., Burri, T., Alt-Epping, P., Engi, M., 2008. Tectonically controlled fluid flow and water-assisted melting in the middle crust: An example from the Central Alps: Lithos 102, 598-615.

Bollinger, L., Janots, E., 2006. Evidence for Mio-Pliocene retrograde monazite in the Lesser Himalaya, far western Nepal: Eur. J. Mineral. 18, 289-297.

Catlos, E. J., Harrison, T. M., Manning, C. E., Grove, M., Rai, S. M., Hubbard, M. S., Upreti, B. N., 2002. Records of the evolution of the Himalayan orogen from *in situ* Th-Pb ion microprobe dating of monazite: Eastern Nepal and western Garhwal: J. Asian Ear. Sci. 20, 459-479.

Clarke, D. B., 1992. Granitoid Rocks, Chapman and Hall. London.

Copeland, P., Parrish, R. R., Harrison, T. M., 1988. Identification of inherited radiogenic Pb in monazite and its implications for U-Pb systematic: Nature 333, 760-763.

Cottle, J. M., Searle, M. P., Horstwood, M. S. A., Waters, D. J., 2009. Timing of midcrustal metamorphism, melting, and deformation in the Mount Everese egion of Southern Tibet revealed by U(-Th)-Pb geochronology: J. Geology 117, 643-664.

Foster, G., Kinny, P., Vance, D., Prince, C., Harris, N., 2000. The significance of monazite U-Th-Pb age data in metamorphic assemblages; a combined study of monazite and garnet chronometry: Ear. Plan. Sci. Lett. 181, 327-340.

Foster, G., Gibson, H. D., Parrish, R., Horstwood, M., Fraster, J., Tindle, A., 2002. Textural, chemical and

isotopic insights into the nature and behaviour of metamorphic monazite: Che. Geo. 191, 183-207.

Goscombe, B., Gray, D., Hand, M., 2006. Crustal architecture of the Himalayan metamorphic front in eastern Nepal: Gond. Res. 10, 232-255.

Harrison, T. M., Grove, M., McKeegan, K. D., Coath, C. D., Lovera, O. M., Le Fort, P., 1999. Origin and episodic emplacement of the Manaslu intrusive complex, central Himalaya: J. Petr. 40, 3-19.

Harrison, T. M., Catlos, E. J., Montel, J-. M., 2002. U-Th-Pb dating of phosphate minerals: Rev. Mineral. 48, 523-558.

Hodges, K., Bowring S., Davidek, K., Hawkins, D., Krol, M., 1998. Evidence for rapid displacement on Himalayan normal faults and the importance of tectonic denudation in the evolution of mountain ranges. Geology 26, 483-486.

Hodges, K. V., 2000. Overview: Tectonics of the Himalaya and southern Tibet from two perspectives. Geol. Soc. Ame. Bulletin 112, 324-350.

Inger, S., Harris, N., 1993. Geochemical constraints on leucogranite magmatism in the Langtang Valley, Nepal Himalaya: J. Petr. 3, 345-368.

Kato, T., 2005. New accurate Bence-Albee a-factors for oxides and silicates calculated from the PAP correction procedure: Geosta. Geoan. Res. 29, 83-94.

Kohn, M. J., Wieland, M. S., Parkinson, C. D., Upreti, N., 2005. Five generations of monazite in Lnagtang genisses: implications for chronology of the Himalayan metamorphic core. J. Met. Geo. 23, 399-406.

Le Breton, N., Thompson, A. B., 1988. Fluid-absent (dehydration) melting of biotite in metapelites in early stages of crustal anatexis: Cont. Min. Petr. 99, 226-237.

Le Fort, P., 1975. Himalayas: The collided range. Present knowledge of the continental arc: Ame. J. Sci. 275-A, 1-44.

Morishita, T., Suzuki, K., 1993. XRF analyses of the Mitsuhashi granite in the Shitara area, Aichi Prefecture: Bull. Nagoya Univ. Furukawa Mus. 9, 77-90 (in Japanese with English abstract).

Murphy, M. A., Harrison, T. M., 1999. Relationship between leucogranites and the Qomolangma detachment in the Rongbuk Valley, south Tibet: Geology 27, 831-834.

Pyle, J. M., Spear, F. S., Wark, D. A., Daniel, C. G., Storm, L., 2005. Contributions to precision and accuracy of monazite microprobe ages: Ame. Mineral. 90, 547-577.

Schärer, U., 1984. The effect of initial ^{230}Th disequilibrium on young U-Pb ages: the Makalu case, Himalaya: Ear. Pla. Sci. Let. 67, 191-204.

Schelling, D., 1992. The tectonostratigraphy and structure of the eastern Nepal Himalaya: Tectonics 11, 925-943.

Simpson, R. L., Parrish, R. R., Searle, M. P., Waters, D. J., 2000. Two episodes of monazite crystallization during metamorphism and crustal melting in the Everest region of the Nepalese Himalaya: Geology, 28, 403-406.

Suzuki K, Adachi M. 1991. Precambrian provenance and Silurian metamorphism of the Tsubonasawa paragneiss in the South Kitakami terrane, Northwast Japan, revealed by the chemical Th-U-total Pb isochron ages of monazite, zircon and xenotime: Geochem. J. 25, 357–76.

Suzuki, K., Adachi, M., Kajizuka, I., 1994. Electron microprobe observations of Pb diffusion in metamorphosed detrital monazites: Ear. Plan. Sci. Let. 128, 391-405.

Suzuki, K., Kato, T., 2008. CHIME dating of monazite, xenotime, zircon and polucrase: Protocol, pitfalls and chemical criterion of possibly discordant age data: Gond. Res. 14, 569-586.

Townsend, K. J., Miller, C. F., D'Andrea, J. L., Ayers, J. C., Harrison, T. M., Coath, C. D., 2000. Low

temperature replacement of monazite in the Ireteba granite, Southern Nevada: Geochronological implications: Chem. Geo. 172, 95-112.

Vidal, P., Cocherie, A., Le Fort, P., 1982. Geochemical investigations of the origin of the Manaslu leucogranite (Himalaya, Nepal): Geochim. Cosmo. Acta 46, 2279-2292.

Viskupic, K., Hodges, K. V., 2001. Monazite-xenotime thermochronometry: methodology and an example from the Nepalese Himalaya. Cont. Min. Petr. 141, 233-247.

Viskupic K., Hodges, K. V., Bowring, S. A., 2005. Timescales of melt generation and the thermal evolution of the Himalayan metamorphic core, Everest region, eastern Nepal: Contrib. Mineral Petrol. 149, 1-21.

Williams, M. L., Jercinovic, M. J., Hetherington, C. J., 2007. Microprobe monazite geochronology: Understanding geologic processes by integrating composition and chronology: Annu. Rev. Ear. Pla. Sci. 35, 137-175.